Multi-scale strategy for modeling macrocracks propagation in reinforced concrete structures

Christian Nader, Pierre Rossi, Jean-Louis Tailhan

Multi-scale strategy for modeling macrocracks propagation in reinforced concrete structures

Christian Nader, Pierre Rossi, Jean-Louis Tailhan

Multi-scale Strategy for Modeling Macrocracks Propagation in Reinforced Concrete Structures

Christian Nader, Pierre Rossi[1], Jean-Louis Tailhan

Institut Français des Sciences et Technologies des Transports, de l'Aménagement et des Réseaux (IFSTTAR), Université Paris-Est

Abstract

This paper introduces a new approach to model cracking processes in large reinforced concrete structures, like dams or nuclear power plants. For these types of structures it is unreasonable, due to calculation time, to explicitly model rebars and steel-concrete bonds. To solve this problem, we developed, in the framework of the finite element method, a probabilistic macroscopic cracking model based on a ulti-scale simulation strategy: the Probabilistic Model for (finite) Elements of Reinforced Concrete (PMERC).

The PMERC's identification strategy is case-specific because it holds information about the local behaviour, obtained in advance via numerical experimentations.

The Numerical experimentations are performed using a validated cracking model allowing a fine description of the cracking processes.

[1] **Corresponding author : Tel.:+ 33 6 80 01 72 26**
E-mail address: pierre.rossi@ifsttar.fr **(Pierre Rossi)**

The method used in the inverse analysis is inspired from *regression algorithms*: data on the local scale would shape the macroscopic model.

Although the identification phase can be relatively time-consuming, the structural simulation is as a result, very fast, leading to a sensitive reduction of the overall computational time.

A validation of this multi-scale modelling strategy is proposed. This validation concerns the analysis of the propagation of a macrocrack in a very large Double Cantilever Beam specimen (DCB specimen usually used in the framework of Fracture Mechanics studies) containing rebars. Promising results in terms of global behaviour, macrocracking information and important reduction in simulation time are obtained.

Keywords

Reinforced concrete structures; Cracking process; Finite Elements; Multi-Scale Modelling Strategy; Probabilistic Approach.

1. Introduction

IFSTTAR, the French Institute of Science and Technology for Transports, Development and Networks, has been developing a probabilistic explicit cracking model since 1987 [1]. The numerical model, originally developed to analyze the cracking of concrete, was more recently enhanced to explicitly take into account the presence of rebars and the bond between rebars and concrete (to model real concrete structures) [2 – 4].

The use of this type of numerical models constitutes a local modelling strategy. They are interesting because they yield reliable and precise information about the cracking process. They can also be used in the framework of numerical experimentations in case there is a lack of experimental data.

Nevertheless, the modelling level they consider becomes inefficient (due to the unreasonably high computational time) when the structures concerned are large or contain a high percentage of rebars, which is the case for almost all complex real-life structures such as dams or nuclear power plants.

Nowadays, there exist other techniques to model cracking in large structures [5 - 8]. They are mainly based on homogenization approach of reinforced concrete. Although these techniques are interesting, they presents two main limitations: they do not give precise information about macrocracks opening and they remain relatively computational time consuming(when large reinforced structures are concerned).

The objective of this work is to propose a more relevant solution which allows (for design offices) to obtain good information about the macrocracking (macrocracks spacing and opening) of a large reinforced concrete structure in a reasonable computational time.

This solution is the Probabilistic macroscopic Model for finite Elements of Reinforced Concrete (PMERC).

The strategy of development of this 3D numerical model its theoretical formulation and its validation are presented, in detail, in this paper.

2. Strategy for developing a PMERC

The strategy has been broken down into distinct steps that map different scales of modelling. The model depends on the dimensions and the configuration of the macro element (total section and number of rebars taken into account in each macro element, for example) which depend on the boundary conditions of the structural problem. The PMERC is thought in terms of its two interconnected components: the macro element itself (the ERC part of the PMERC acronym) defined by its dimensions and configuration, and the probabilistic model (the PM part of the PMERC acronym) describing its behaviour.

A strong assumption is therefore made, which states that the ERC behaves only in tension in the considered direction(s) of reinforcement(s). To be more precise, it is assumed that only one macrocrack appears in each macro element, this macrocrack being oriented perpendicularly to the rebar direction.

The Multi-Scale Modelling Strategy can be summarized as follow:

First step: determination of the fineness of the finite element mesh and of the dimension of the ERC(s)

An elastic simulation of the given structure is performed taking into account the boundary conditions of our problem. 2D or 3D (as required) volume elements are used without describing any reinforcements. This step is necessary to determine the coarsest finite element mesh that would still yield the correct kinematic field. This will set an upper limit on the size of the macro elements. Subsequently, the fineness of the mesh and the optimal ERC(s) (optimal in terms of geometry, size, and ubiquity) are chosen.

Second step: determination of the different tie-beams geometry

One or multiple ERC(s) are now defined – distinct either by their dimensions and/or their composition (position, number, and type of rebars).

Different tie-beam numerical tests, for each ERC, in every direction of reinforcements (numerical experimentation phase) are then defined. The length of these tie-beam specimens has to be sufficient to get a representative cracking pattern (it means a cracking pattern which results in a correct way the number of macrocracks per length of tie-beam).

Third step: numerical simulations of the different tie-beams by using a local modelling approcah

Numerical simulations on the tie-beams are run to get information about cracking and global responses. To that end, validated local models are used: a probabilistic explicit cracking model for concrete and an interface element model for steel-concrete bond (section 4).

Fourth step: determination of the macroscopic model parameters of the different ERCs

Results from the tie-beam simulations (along with some working knowledge) help to deduce, by inverse analysis, the cracking behaviour of the different ERCs. The mechanical macroscopic model and the method used to determine the parameters of the constitutive law are detailed in section 3.

Fifth step: numerical analysis of the reinforced structure with the macroscopic model

Due to the fact that the macroscopic model used is a probabilistic one, it is important to perform several simulations (Monte-Carlo approach) to get information about the scattering related to the structural behaviour. By this way, it is then easy to perform safety analysis of this structure.

The so-called FE^2 methods were developed and used, in the past, by others researchers [9, 10]. They are based on the hierarchical, bottom-up one-way coupled description of the material using the finite element methods in both scales and computational homogenization procedures at the low scale. The main differences between their work and this one can be summarized as follow:

- They treated only the problem of material behaviour and not that of reinforced concrete structures behaviour.
- They did not develop probabilistic approaches.
- They did not precisely treat the problem of cracks opening.

3. PMERC theory

The model is required to have the following features:

- The ability to get information on macro-cracks spacing and openings in a large reinforced concrete structure.
- A probabilistic modelling to allow for a statistical analysis of the structural behaviour via a Monte Carlo approach (reliability analysis of the structure).

3.1. Formulation of the model

To achieve our objectives, and still save on calculation time, the model has to be simple. Therefore, some strong assumptions are made:

- At the global structural scale, our scale of interest, the concrete part of the PMERC breaks in a brittle way. Therefore, the composite element is assumed to have an elastic brittle behaviour. Only failure criteria in tension and in shear are considered (the criterion for shear is only relevant when compressive stress fields are involved). These criteria are applied at the centre of gravity of the ERC. As for concrete alone, the values of the tensile and shear strengths of the ERC are considered as random values. At the difference of concrete alone, the distribution function chosen for the ERC is not a Weibull one but a lognormal one is (it is an arbitrary choice).
- Once the matrix is broken, the stresses in the element plunge to zero – a reasonable approximation at the scale of structural elements. Then, immediately after, the rebars intervene mechanically. This requires a new evaluation of the coefficients of the stiffness matrix of the ERC – in the direction parallel to the rebars. The new values of these

coefficients are associated with the stiffness of the rebars and the phenomenon of tension stiffening. They are considered as random values. It is to take into account the mechanical scattering related to the tension stiffening phenomenon. A lognormal distribution function is chosen arbitrary for these random values. As a matter of fact, a Weibull distribution function is not physically relevant for the post-cracking behavior of the ERC.

- The PMERC accounts for the plastic behaviour of the rebars in the studied direction: when the linear elastic strain limit of the steel is reached at the center of gravity of the ERC, its behaviour would be represented by an elasto-perfectly-plastic model. We chose, for simplicity, to simulate this behaviour with a damage model (permanent deformations due to the yield of the rebars are not considered). This simplification is only possible if monotonically increasing loadings are involved, which the case in this work.

As explained before, the macro-element is reinforced in only one direction. It can therefore be considered as an orthotropic material. A fixed orthogonal reference frame is locally placed with its direction 1 as the one of the reinforcement. Next, in agreement with homogenization techniques, it is considered that the element consists of a smeared orthotropic material. Thus the elastic 3D constitutive law is:

$$\boldsymbol{\sigma} = \boldsymbol{H}.\boldsymbol{\varepsilon} \tag{1}$$

$$\begin{bmatrix}\sigma_{11}\\ \sigma_{22}\\ \sigma_{33}\\ \sigma_{12}\\ \sigma_{13}\\ \sigma_{23}\end{bmatrix} = \frac{1}{\Delta}\begin{bmatrix} \frac{(1-\vartheta_{23}.\vartheta_{32})}{E_2E_3} & \frac{(\vartheta_{21}-\vartheta_{31}.\vartheta_{23})}{E_2E_3} & \frac{(\vartheta_{31}-\vartheta_{21}.\vartheta_{32})}{E_2E_3} & 0 & 0 & 0 \\ \frac{(\vartheta_{12}-\vartheta_{13}.\vartheta_{32})}{E_1E_3} & \frac{(1-\vartheta_{31}.\vartheta_{13})}{E_1E_3} & \frac{(\vartheta_{32}-\vartheta_{31}.\vartheta_{12})}{E_1E_3} & 0 & 0 & 0 \\ \frac{(\vartheta_{13}-\vartheta_{12}.\vartheta_{23})}{E_1E_2} & \frac{(\vartheta_{23}-\vartheta_{13}.\vartheta_{21})}{E_1E_2} & \frac{(1-\vartheta_{12}.\vartheta_{21})}{E_1E_2} & 0 & 0 & 0 \\ & & & G_{12}.\Delta & 0 & 0 \\ & SYM & & 0 & G_{13}.\Delta & 0 \\ & & & 0 & 0 & G_{23}.\Delta \end{bmatrix}\begin{bmatrix}\varepsilon_{11}\\ \varepsilon_{22}\\ \varepsilon_{33}\\ 2\varepsilon_{12}\\ 2\varepsilon_{13}\\ 2\varepsilon_{23}\end{bmatrix} \quad (2)$$

$$\Delta = \frac{E_1E_2E_3}{1-\vartheta_{23}.\vartheta_{32}-\vartheta_{31}.\vartheta_{13}-\vartheta_{12}.\vartheta_{21}-2.\vartheta_{23}.\vartheta_{31}.\vartheta_{12}} \quad (3)$$

Assumptions are made concerning the elastic coefficients of the orthotropic stiffness matrix $\boldsymbol{H}$:

- $\boldsymbol{E_1}$: Young modulus in the direction of the rebars; calculated as a result of the average Young modulus of both the concrete and the rebars according to the rule of mixtures (Voigt model).
- $\boldsymbol{E_2 = E_3}$: Young modulus of the concrete (an approximation).
- $\boldsymbol{\vartheta_{12} = \vartheta_{13} = \vartheta_{23} = \vartheta_{32}}$: Poisson's ratio of the concrete.
- $\frac{\boldsymbol{\vartheta_{21}}}{\boldsymbol{E_2}} = \frac{\boldsymbol{\vartheta_{12}}}{\boldsymbol{E_1}}$; $\frac{\boldsymbol{\vartheta_{31}}}{\boldsymbol{E_3}} = \frac{\boldsymbol{\vartheta_{13}}}{\boldsymbol{E_1}}$ (to ensure that $\boldsymbol{H}$ is symmetric).
- G_{23}: Shear modulus of plain concrete (an approximation)
- $G_{12} = G_{13}$: Shear modulus that takes into consideration the presence of the rebars in the volume of the element with respect to the rule of mixtures (Voigt model).

When failure criteria are applied in tension (Rankine) or in shear (Tresca) the failure limit is reached and the stresses are then immediately picked up by a reduced elastic matrix representing the remaining contribution of the steel bars with some residual action from the

surrounding concrete (in the form of friction). Some terms of the initial elastic constitutive relation (1 and 2) are then affected by a reduction coefficient, β:

$$\boldsymbol{\sigma} = \boldsymbol{H}'.\boldsymbol{\varepsilon} \tag{4}$$

$$\begin{bmatrix}\sigma_{11}\\ \sigma_{22}\\ \sigma_{33}\\ \sigma_{12}\\ \sigma_{13}\\ \sigma_{23}\end{bmatrix} = \frac{1}{\Delta}\begin{bmatrix} \beta\frac{(1-\vartheta_{23}.\vartheta_{32})}{E_2E_3} & \beta\frac{(\vartheta_{21}-\vartheta_{31}.\vartheta_{23})}{E_2E_3} & \beta\frac{(\vartheta_{31}-\vartheta_{21}.\vartheta_{32})}{E_2E_3} & 0 & 0 & 0 \\ \beta\frac{(\vartheta_{12}-\vartheta_{13}.\vartheta_{32})}{E_1E_3} & \frac{(1-\vartheta_{31}.\vartheta_{13})}{E_1E_3} & \frac{(\vartheta_{32}-\vartheta_{31}.\vartheta_{12})}{E_1E_3} & 0 & 0 & 0 \\ \beta\frac{(\vartheta_{13}-\vartheta_{12}.\vartheta_{23})}{E_1E_2} & \frac{(\vartheta_{23}-\vartheta_{13}.\vartheta_{21})}{E_1E_2} & \frac{(1-\vartheta_{12}.\vartheta_{21})}{E_1E_2} & 0 & 0 & 0 \\ & & & G_{12}.\Delta & 0 & 0 \\ & SYM & & 0 & G_{13}.\Delta & 0 \\ & & & 0 & 0 & G_{23}.\Delta \end{bmatrix}\begin{bmatrix}\varepsilon_{11}\\ \varepsilon_{22}\\ \varepsilon_{33}\\ 2\varepsilon_{12}\\ 2\varepsilon_{13}\\ 2\varepsilon_{23}\end{bmatrix} \tag{5}$$

β could also be viewed as an anisotropic damage variable. Actually, the whole process envolving the drop in stresses, and the contribution of steel until yielding, can be numerically represented by a damage formulation:

σ_r is the constraint value in direction 1 (that of the reinforcement) right after the drop resulting from the failure criterion being reached. $E_1^{'}$ is the residual stiffness in direction 1. σ_r and $E_1^{'}$, along with σ_t^{cri} (the tensile strength of the unckracked element) are the unknown model parameters.

The drop from σ_t^{cri} to σ_r can be the result of an initial anisotropic damage constant D_{ini}^c, where:

$$D_{ini}^c = 1 - \frac{\sigma_r}{\varepsilon_{0_1}.E_1} \tag{6}$$

ε_{0_1} here is the state of strain in direction 1 after the brittle failure of the element. So we assume that the cracking of the element has damaged it and we now have established a damage variable D^c with a lower bound D_{ini}^c.

The stresses are then picked up by the reduced elastic matrix represented by $E_1^{'} = \beta E_1 = (1 - D^c)E_1$ (physically the steel bars with some residual friction from the surrounding concrete).

D^c is considered a state variable, thus its evolution has to verify the following conditions:

$$\begin{cases} \dot{D}^c \geq 0 \\ D^c = \max\left(D_0^c, D^c\right) \end{cases} \tag{7}$$

Where D_0 is the initial damage state, and D is the actual damage state. The initial damage threshold (D_{ini} in this case) is established when the failure criterion is reached in the direction of the reinforcement. One the element is declared as cracked (failure criteria reached) the damage evolution is then given by the following relations:

$$\begin{cases} D^c(\tilde{\varepsilon}) = D_{ini}^c \;\; ; \;\; \tilde{\varepsilon} \leq \varepsilon_{0_1} \\ D^c(\tilde{\varepsilon}) = 1 - \dfrac{\sigma_r + E_1'\left(\tilde{\varepsilon} - \varepsilon_{0_1}\right)}{E_1\tilde{\varepsilon}}; \;\; \varepsilon_{0_1} < \tilde{\varepsilon} \leq \dfrac{\sigma^p - \sigma_r}{E_1'} + \varepsilon_{0_1} \\ D_{max}^c = \text{constant value if } \tilde{\varepsilon} \geq \dfrac{\sigma^p - \sigma_r}{E_1'} + \varepsilon_{0_1} \end{cases} \tag{8}$$

Where $\tilde{\varepsilon} = \langle \varepsilon_1 \rangle_+$ ($\langle \cdot \rangle_+$ is the positive part of $(\cdot)$). This behavior is held until the (predetermined) yield limit of the steel is reached.

To represent the plastic behavior of the reinforcements all it is needed to do is to update the damage model. Note that it is not saying that plasticity is the same as damage, it is just used the convenience of the damage formulation to represent the plastic behavior of the macro-element. Once the stresses in the element reach the yield limit of the steel, the behavior of the element will be represented as follows:

$$\boldsymbol{\sigma} = (1 - D^p)\boldsymbol{H}'.\boldsymbol{\varepsilon} \tag{9}$$

$$\dot{D}^p \geq 0$$

234

235 And the damage evolution is now given by:

$$D^p(\tilde{\varepsilon}) = 1 - \frac{\sigma^p - \sigma_r + E_1'\varepsilon_{0_1}}{E_1'\tilde{\varepsilon}};\ \ \tilde{\varepsilon} > \frac{\sigma^p - \sigma_r}{E_1'} + \varepsilon_{0_1} \tag{10}$$

236

237 At this stage, the model still carries two unknown parameters: the tensile strength of the
238 uncracked elementσ_t^{cri}, and the residual stiffness in direction 1, $E_1' = \beta E_1$ (stiffness of the
239 elastic steel bars in this direction, plus friction with the cracked concrete matrix). Lognormal
240 distribution functions are assigned to both σ_t^{cri} andE_1'.
241 It can be noted that the mean shear strength is assumed to be equal to the half of the
242 compressive strength, and its standard deviation is equal to that of the tensile strength.
243 If the fourth step of the numerical strategy (see section 2) is considered, the resulting force-
244 displacement curve from the global approach has to be fitted to that of the local approach
245 (numerical experimentations) on the tie-beam tests. The best fit will determine the different
246 parameters for both distribution functions. Consequently, this classifies the methodology as
247 an optimization problem. The optimization tool most suited for the problem is the Response
248 Surface Method (RSM) [11]. RSM is a way to explore the effect of operating conditions (the
249 factors/parameters) on the response variable, y. In the present case, y is the surface area of the
250 complex polygon outlined by the real force/displacement curve and the fitted curve. To
251 calculate the surface area of this highly irregular and self-intersecting polygon the Bentley–
252 Ottmann algorithm [12] is used. As the unknown response surface of y is mapped out, the
253 process continues as close as possible towards an optimum (i.e. the minimum value of the
254 considered area), taking into account any constraints.

At the end of this step, the parameters that minimize y are the ones which are input into the model for the final calculations.

To summarize, the parameters involved in the process of creating the complete mechanical model for a given ERC (given concrete and reinforcements) are:

- The parameters of the probabilistic explicit or semi-explicit cracking model of the concrete.
- The values of C and δ_t^{cri} for the interface elements (steel-concrete bond model) which allows us to perform the correct numerical simulations of the tie-beam test(s). The results from these numerical simulations constitute the starting point for fitting the values of the parameters of the ERC.
- The elastic orthotropic stiffness matrix of the ERC, assembled with the help of some intuitive hypotheses and the rule of mixtures.
- The parameters of the lognormal distribution function for the tensile strength of the chosen ERC (in the direction of rebars).

  The average value of the tensile strength of a given ERC is necessarily smaller than the one for the same volume of plain concrete; the presence of rebars introduces an extra level of heterogeneity (concentration of stresses around the rebars) that promotes fracture initiation.
- The parameters of the lognormal distribution function for the shear strength of the ERC. The mean value is equal to half the average compressive strength of the considered concrete. Its deviation is considered identical to that of the ERC's tensile strength.
- The parameters of the lognormal distribution function of the residual stiffness of the ERC after cracking.

279 Figure 4 summarizes the model's pre and post cracking behaviour in the direction of the
280 rebars.
281
282 **3.2. Probabilistic cracking models**
283
284 The probabilistic model was first developed at IFSTTAR (formerly LCPC) by Rossi [1, 13]
285 and more recently improved by Tailhan et al. [14]. It describes the behaviour of concrete via
286 its two major characteristics: heterogeneity, and sensitivity to scale effects [15]. The physical
287 basis of the model (presented in detail in [1, 13]) can be summarized as follow:
288 1) The heterogeneity of concrete is due to its composition. The local mechanical
289 characteristics (tensile strength f_t, shear strength τ_c) are randomly distributed.
290 2) The scale effects are a consequence of the heterogeneity of the material. The mechanical
291 response directly depends on the volume of material that is stressed.
292 3) The cracking process is controlled by defects in the cement paste, by the heterogeneity of
293 the material, and by the development of tensile stress gradients.
294 4) The following points specify how the numerical model accounts for these physical
295 evidences:
296 5) The model is developed in the framework of the finite element method, each element
297 representing a given volume of (heterogeneous) material.
298 6) The tensile strength is distributed randomly on all elements of the mesh using a Weibull
299 distribution function whose characteristics depend on the ratio: *volume of the finite*
300 *element/volume of the largest aggregate*, and the compressive strength (as a good
301 indicator of the quality of the cement paste). The volume of the finite element depends on
302 the mesh, while the volume of the largest aggregate is a property of the concrete [1, 13,
303 14].

The Weibull distribution function is the best to take into account the rupture in tension of a brittle and heterogeneous material as concrete.

7) The shear strength is also distributed randomly on all elements using a distribution function: (1) its mean value is independent of the mesh size and is assumed equal to the half of the average compressive strength of the concrete and (2) its deviation depends on the element's size, and is the same (for elements of same size) as that of the tensile strength.

8) Concerning the cracks representation, two approaches are proposed:

a) First approach: explicit cracking

The cracks are explicitly represented by non-linear interface elements of zero thickness. These elements connect volume elements representing un-cracked plain concrete. Failure criteria of Rankin in tension and Tresca in shear (to take into account cracks generated by compressive stresses [16]) are used. As far as tensile or shear stresses remain lower than their critical values, the interface element ensures the continuity of displacements between the nodes of the two neighboring volume elements. The material cell gathering these two volume elements and the interface element remains therefore elastic. Once one of the preceding failure criteria is reached, the interface element opens and an elementary crack is created. The tensile and shear strengths as well as the normal and tangential stiffness values, related to this interface element, become equal to zero [1, 13, 14]. In case of crack re-closure, the interface element recovers its normal stiffness and follows a classical Coulomb's law [16].

Note that in this modelling approach, the creation and the propagation of a crack is the result of the creation of elementary failure planes that randomly appear and can coalesce to form the macroscopic cracks (Figure 1).

329 *b) Second approach: semi-explicit cracking*

330 The cracks are modeled using linear volume elements. At the finite element scale, the
331 energetic effect associated to the elementary cracking process is represented through a simple
332 isotropic damage law with a single scalar parameter [17] (the model is presented in details in
333 [18]). A probabilistic energetic regularization is also retained.

334 Without going into details of numerical implementation of the model, its main features can be
335 summarized as follows:

336 • A bilinear stress–strain relationship is used to represent elementary cracking (Figure
337 2). The elementary dissipative process (i.e. crack propagation inside the FE itself)
338 starts when the major principal stress at a given Gauss point equals the material tensile
339 strength. Dissipation is then driven by the positive part of the projection of the strain
340 along the normal direction of the major principal stress. When the total energy
341 available for the FE is dissipated, it is declared cracked and its elementary stiffness
342 matrix is set to zero [18]. This allows avoiding stress-locking phenomena.

343 • The model is numerically implemented using a rotating crack approach [20, 21].
344 During the dissipative phase, the stress is allowed to evolve according to any changes
345 in the stress state in the material.

346 • Differently from smeared-cracking approaches [21-23], no additive decomposition is
347 introduced in the constitutive law to distinguish between elastic deformation and crack
348 contributions. An elementary crack is supposed to exist only after the condition the
349 damage parameter equal 1 is achieved [18]. The elementary crack opening is then
350 computed from the projection of the elementary displacements along the normal
351 direction of the major principal stress.

352 • For sake of simplicity, crack re-closure is not explicitly treated. The model assumes
353 that the dissipative process does not influence the elementary stiffness in compression.

So, for reclosed cracks, the elementary stiffness matrix in compression is completely recovered while the elementary tensile strength is set to zero.

The constitutive law of the model is completely defined by two parameters: the tensile strength and the volumetric density of dissipated energy. An energetic regularization technique allows computing the volumetric density of dissipated energy from the surface cracking energy by dividing this last energy by an elementary characteristic length [24]. This elementary characteristic length, l_e, is here computed from elementary volume, V_e, as $l_e = V_e^{1/3}$. More complex definitions are possible, depending on the FE shape and the order of interpolation of the displacement field. This choice can influence the predicted crack paths, however due to the probabilistic aspects of the model this effect is strongly reduced. The volumetric density of dissipated energy is defined element-by element according to spatially uncorrelated lognormal statistical law [25]. This choice of a lognormal statistical law is an arbitrary one (the use of a Weibull law is not relevant anymore as for the tensile strength distribution due to the fact that, in this approach, the rupture is no more considered as perfectly brittle). As for the tensile strength parameters, the standard deviation related to the volumetric density of dissipated energy depend on the elementary volume. In contrary, the mean value of the energy distribution is assumed independent of elementary volume. Its value is estimated as 2γ where γ is the specific fracture energy per unit area (which is an intrinsic material parameter) according Griffith's theory [26].

Note that in this modelling approach, the creation and the propagation of a crack is the result of the creation of elementary holes that randomly appear and can coalesce to form the macroscopic cracks.

It is important to underline that:

- The first approach gives a more precise and relevant information about the cracking description and the cracking process but is a lot of more simulation time consuming than the second approach.
- Due to this problem of simulation time consuming, the second approach is recommended to perform 3D simulations.

3.3. Concrete/steel bond model

Two modelling approaches were introduced to model the concrete-rebar bond [2, 3, and 4]:

- The concrete-rebar bond is represented by interface elements. Their behaviour is described with a simple deterministic damage model with only two parameters, cohesion and slip (i.e. relative tangential displacement between steel and concrete).
- The notches/indentations are explicitly modeled along the whole length of the rebar with a perfect bond between concrete and rebar.

The first approach needs to have experimental information about this steel-concrete bond in order to perform inverse analysis for determining the values of the interface model parameters.

The second approach is used only when you have not any experimental information about this steel-concrete bond. It is more local than the first one but also more time consuming.

The interface element for modeling the steel-concrete bond

Its role is to:

401 - Ensure the displacement continuity between the concrete and the steel before the slip
402 of the interface and before the cracking of the concrete, thus ensuring the transfer of
403 stresses between steel and concrete.
404 - Represent the macroscopic mechanical effect of the rebar at the ribs – which is not
405 explicitly represented in the mesh.
406 - Simulate a local failure between steel and concrete along the rebar resulting from a
407 loss of the local adhesion due to shear cracking.
408 - Simulate the local friction between the concrete and the steel after the interface
409 failure.
410
411 The model is implemented in 2D and 3D [2, 3]. It considers the concrete-rebar bond as a
412 material zone that progressively degrades in shear (the tensile failure is neglected). Prior to
413 total failure, stresses are continuously transmitted through the interface.
414 The interface model is based on a damage model that maintains a constant level of stress
415 when the critical shear has been reached (Figure 3). When the relative tangential
416 displacement between the concrete and the rebar exceeds a critical value, the interface
417 element is declared broken [27]. After failure, a Mohr-Coulomb type of friction behaviour is
418 maintained.
419 The interface model is deterministic. This is a valid approximation because the cracking
420 process around the rebar is governed by the presence of the ribs (rather than the heterogeneity
421 of concrete) [28].
422 Only the values of the maximum shear stress, and of the tangential critical relative
423 displacement, have to be determined. It is realized by performing a numerical inverse
424 analysis, it means by fitting tie-beam test results obtained with the rebar and the concrete
425 concerned [2, 4].

In the framework of the proposed numerical modelling strategy, only 2D interface elements are used. As a matter of fact, it should be unrealistic, due to computational time considerations, to perform 3D numerical analysis of tie-beam tests. This assumption that a 2D numerical analysis (plane stresses conditions) of a 3D tie-beam test is acceptable has been clearly justified and validated in previous works [2, 4]

4. Example of application of the Multi-Scale Modelling Strategy

As validation example, a structural problem that has been previously studied by the authors has been chosen [29-31]. This structural problem concerns the analysis of the macrocrack propagation in a Double Cantilever Beam (DCB) concrete specimen. This type of specimen and study are very common in the framework of Linear Fracture Mechanics theory. The specificity of the specimen concerned by this paper is related to two points: the first one concerns the fact that the dimensions of the specimen are very (unusually) important (3.5 meters length and 1.1 meters width) and the second concerns the fact that the specimen contains rebars along of the potential propagation of the macrocrack [29].

So, this structural problem is clearly related to the propagation of a macrocrack over a long distance and crossing rebars. It is an interesting case in relation with the spirit of the modelling strategy approach presented in this paper.

To make a comparison between the local approach performances with the macroscopic approach performances, it has also been decided to model the DCB specimen behaviour in the framework of the local approach. As, it is not reasonable (due to simulation time

450 considerations), to use a 3D approach to achieve this local modelling, a 2D approach is
451 performed.
452
453 **4.1. Some details about the validation test**
454
455 The dimensions of the specimen and the loading conditions related to the test are presented in
456 Figure 5. The steel bars used were ribbed ones with 6 mm diameter. The distance between the
457 rebars was 10 cm and the first rebar was located at 30 cm from the front tip of the notch
458 (Figure 6).
459 Note that the specimen contained a narrowed section in its center part to force the propagation
460 of the macrocrack along this reduced section (Figure 5). For the same reason and objective,
461 prestressing cables were used and placed along the flanges of the specimen (Figure 5).
462
463 **4.2. Numerical simulations**
464
465 4.2.1. 3D macroscopic approach
466 The first step of the modelling strategy (section 2) is to choose the dimensions of the ERC
467 (dimensions of the "macro-element"). These dimensions have to be relevant in respect to the
468 achievement of a correct kinematic field.
469 In the case of the DCB specimen concerned by this study (figure 5), two points have to be
470 noted:
471 • The first one is that the mesh has to be very fine at the front tip of the notch where only
472 concrete is present (high stresses concentration).

- The second one concerns the part of the specimen where rebars are present. In this part, there are not stresses concentration due to the mechanical acting of the rebars. So, the finite elements can be much larger.
- To evaluate the influence of the dimension of the ERC chosen both on the relevancy of the numerical results (by comparison with the experimental result) and the computational time, it has been decided to consider 3 types of ERC dimensions:
  - ERC1: Length (L): 10 cm, High (H): 10 cm, Thickness (T): 10 cm.
  - ERC2: L: 10 cm, H: 5 cm, T: 10 cm.
  - ERC3: L: 10 cm, H: 20 cm, T: 10 cm.

It can be noted that**:**

- ERC1 and ERC2 contain one rebar.
- ERC3 contains two rebars.
- The thickness of the 3 ERC is the same and equal to 10 cm, because it is assumed that the macrocrack will pass along the narrowed section of the DCB specimen. It means that, in this zone, only one ERC is present in the thickness of the DCB specimen

In Figure 7 is presented (as example) the 3D finite elements meshes containing, ERC1. In Figure 8 is presented 2D cuts of the three different 3D finite elements meshes (with ERC1, ERC2 and ERC3). It can be noted that for the finite element mesh related to the use of ERC2, it is necessary to introduce also finite elements representing only concrete.

The second step of the modelling strategy is related to the choice of the tie beam configurations (3 configurations, one by ERC), on which the inverse approach permitting to

498 determine the parameters of the macroscopic mechanical model associated to each ERC has
499 to be performed. Considering Figure 7, the 3 tie-beams chosen for performing 2D (plane
500 stresses conditions) simulations with the local approach have the following dimensions:

501 - ERC1: tie-beam 1 (TB1) with a high of 10 cm and a length of 140 cm.
502 - ERC2: TB2 with a high of 5 cm and a length of 140 cm.
503 - ERC3: TB3 with a high of 20 cm and a length of 140 cm.

504

505 The third step of the modeling strategy is, now, to perform the numerical simulations of the
506 different tie-beams. Normally, to perform the numerical simulation in the framework of the
507 local approach, the best way (related to computational time considerations, see section 4) to
508 model the concrete/steel bond is to use interface elements.
509 The problem is that no tie-beam tests were performed in parallel to DCB test. So, it is not
510 possible to determine the parameters of the interface element behaviour law.
511 The solution is to use the second way to model this steel-concrete bond (see section 4.2), it
512 means to explicitly model all the notches/indentations of the rebars. Of course, this solution is
513 computational time consuming, but it consists to replace experimental tests, which are also
514 time consuming, by numerical tests.
515 The three 2D finite elements meshes related to the 3 numerical tie-beams (local approach and
516 2D stresses plane conditions) are presented in Figure 9.
517 Concerning the probabilistic model used for the concrete, the semi-explicit approach is
518 chosen (section 4.1).
519 Concerning the modeling of the rebars behaviour, a classical Von Mises law (perfect
520 plasticity) is chosen.
521 The parameters values related to the concrete and the steel models are given in Table 1.

522 Figures 10, 11 and 12 present examples of cracking process obtained with the three numerical
523 tie-beam tests.
524
525 The fourth step consists, now, to determine, by inverse approach, the parameters values
526 related to the macroscopic model.
527 Figure 13 presents the three 3D finite elements meshes chosen to model the three tie-beams in
528 the framework of the macroscopic approach.
529 Figures 14, 15 and 16 present the force-displacement curves obtained with the local and the
530 macroscopic approaches respectively for the three tie-beams.
531 Table 2 gives the values of the material parameters used in the framework of the macroscopic
532 model to get the results summarized by the Figures 14 to 16.
533
534 The fifth step of the modelling strategy consists, finally, to model the cracking behaviour and
535 the global behaviour of the DCB specimen using the results obtained with the modelling of
536 the three tie-beams.
537 The crack mouth opening displacement (CMOD) versus loading curves related to the three
538 3D meshes are presented in Figures 17 to 19.
539 It can be noted that:
540 • As the macroscopic model is a probabilistic one, several numerical simulations are
541 performed in relation with each 3D mesh.
542 • In each figure is reported the experimental curve (one test was performed [27])
543
544 An example of crack propagation using the macroscopic approach is presented in Figure 20.
545 To make a comparison between the local approach performances with the macroscopic
546 approach performances, it has been decided to model the DCB specimen behaviour in the

547 framework of the local approach. As, it is not reasonable (due to simulation time
548 considerations), to use a 3D approach to achieve this local modelling, a 2D approach is
549 performed.
550
551 4.2.2. 2D local approach
552 The first step of the 2D local approach is to determine the values of the parameters related to
553 the concrete/steel bond model using interface elements (section 3.2). As a matter of fact, it is
554 not still reasonable to perform the 2D modelling of the DCB specimen by representing the
555 ribs of the rebars (as for the tie-beam).
556 To get these values, the way chosen is to perform an inverse approach (fitting approach) as
557 proposed, realized and validated in [2-4]. To achieve this inverse approach, the 2D numerical
558 simulations performed with the TB1 are considered as the reference results (Figures 7 and
559 14).
560 The values of the parameters related to the concrete/steel bond model using interface
561 elements are given in Table 3 (obtained from the inverse approach).
562 Figure 21 presents the 2D (plain stresses conditions) finite element mesh used to model the
563 DCB specimen with the local approach.
564 Concrete is modeled by using the semi-explicit approach (see section 3.1).
565 The values of all the parameters involved in the numerical simulations (several numerical
566 simulations are performed, the modelling of the concrete cracking being probabilistic) are
567 those given in Tables 1 and 3.
568 Figure 22 presents the CMOD versus loading curves related to the numerical simulations. The
569 experimental curve is also reported in the figure.
570 Figure 23 presents an example of cracking process obtained with the 2D local modelling.

571 It is now possible to analyze all the results obtained with all (2D and 3D) numerical
572 simulations and to compare them.
573
574 **4.3. Analysis of the results and discussion**
575
576 This analysis and discussion is based on Figures 17 to 20 and 22 to 23.
577 A look of these figures leads to the following comments:
578 • The macroscopic approach (with the three different macro-elements) gives good
579 enough results in terms of global behaviour of the DCB specimen (in comparison with
580 the experimental result). It can be noted, however, that larger are the macro-elements,
581 larger is the difference between the experimental result and the numerical simulations
582 ones. It is an expected result. As a matter of fact, the numerical homogenization,
583 linked to the numerical strategy of modelling proposed in this work, has to lead to a
584 lost of precision of the information obtained (it is the price to pay).
585 • The local approach leads to a more scattered global behaviour of the DCB specimen
586 than the macroscopic approach.. It is still a normal and expected result. As a matter of
587 fact, the numerical homogenization linked to the building of a macro-element leads,
588 obviously, to a kind of smoothing of the mechanical heterogeneities related to the
589 cracking process of a reinforced concrete.
590 • The local approach is capable to give detailed information about the cracking process,
591 it means, microcracks creation accompanying the tortuous propagation of the
592 macrocrack. It is always an expected result.
593
594 So, now, it is capital to make the comparison related to the computational time linked to the
595 use of each approach. To do that, it has been chosen to consider only the computational time

(average values related to the several simulations performed) related to the crack propagation in the zone where the rebars are present.

This comparison is summarized in Table 4.

A look of this Table 4 leads to the following comments:

- To model the same crack propagation length, the local approach spends ten times more computational time than the global one.
- The fact to consider a macro-element with one or two rebars does not lead to a significant difference concerning the computational time.
- The fact to model the concrete cracking alone between the cracking of the macro-elements leads to multiply by two the computational time.

In fact, to be fully precise, it is important to take into account the simulation time linked to the numerical tests on tie-beams. If it is done, the total simulation time to perform the 3D analysis of the DCB specimen is around ***26 hours***. It could be considered as too important in view of the initial objective of this work, it means to propose an approach compatible with design offices work. But, it should not be forgotten that this simulation time devoted to the numerical tests replaces real experimental tests which should take more time to be performed.

5. Conclusions and perspectives

A multi-scale strategy to develop a Probabilistic Model for Elements of Reinforced Concrete (PMERC) is introduced in this paper. This multi-scale strategy consists in building a macro model from numerical experimentations using validated local ones: the probabilistic explicit

621 or semi-explicit cracking model for concrete and the interface element model with a Mohr-
622 Coulomb law for steel/concrete bond.
623 As a validation of this Multi-Scale Modelling Strategy, a previous experimental study related
624 to the crack propagation in a very large DCB specimen is proposed. The 3D numerical
625 simulations show that the scientific approach proposed is promising: the global behaviour of
626 the structure is correctly predicted and the macro-cracking pattern is consistent with results
627 given by the local approach (only precise information about the tortuosity of the macrocrack
628 propagation and the microcracks appearance is lost with the macroscopic approach).
629 The main objective of the PMERC is to reduce the massive computational time required to
630 get information about the cracking process in large structures. It can be considered that this
631 objective is reached in the considered example. These results could still be improved and the
632 gain in computational time would be even more acute for larger structures
633 As perspectives go, it is now important to validate the proposed strategy on larger and real-
634 life structures. It is also necessary to consider the situation where the rebars are positioned in
635 two or more directions. It is also important to emphasize that the strategy proposed in this
636 paper, which consists in changing scale of analysis by changing the numerical modelling
637 scale, can be used in the framework of more sophisticated mechanical models than those
638 implemented in the present work. For that, it is essential for the local scale models chosen to
639 have a strong physical relevance and to be fully validated.
640
641
642
643
644

6. Acknowledgement

The authors gratefully acknowledge the funding support from France's National Research Agency through the "MACENA" project (ANR-11-RSNR-012).

7. References

1. Rossi, P., and Richer, S, Numerical modelling of concrete cracking based on a stochastic approach, *Materials and Structures* 20.5 (1987): 334-337.
2. Phan, T. S., et al., Numerical modeling of the rebar/concrete interface: case of the flat steel rebars, *Materials and structures* 46.6 (2013): 1011-1025.
3. Phan, T. S., Tailhan, J-L and Rossi, P., 3D numerical modelling of concrete structural element reinforced with ribbed flat steel rebars."Structural Concrete 14.4 (2013): 378-388.
4. Phan, T. S., Rossi, P. and Tailhan, J-L.,Numerical modelling of the concrete/rebar bond, *Cement and Concrete Composites* 59 (2015): 1-9.
5. Andriotis, Ch, Gkimousis, I. and Koumousis, V., Modeling Reinforced Concrete Structures Using Smooth Plasticity and Damage Models, *Journal of Structural Engineering* (2015): 04015105.
6. Combescure, Ch., Dumontet, H. and Voldoire F., Homogenized constitutive model coupling damage and debonding for reinforced concrete structures under cyclic solicitations, *International Journal of Solids and Structures* 50.24 (2013): 3861-3874.

669 *7.* Huguet, M. et al., Homogenized global nonlinear constitutive model for RC panels under
670 cyclic loadings, *11th World Congress on Computational Mechanics (WCCM XI), At*
671 *Barcelona, Spain* (2014).
672 8. Sun, B., Xuan W, and Zhaoxia L., Meso-scale image-based modeling of reinforced
673 concrete and adaptive multi-scale analyses on damage evolution in concrete structures,
674 *Computational Materials Science* 110 (2015): 39-53.
675 9. Oliver, J. et al., Mult-scale (FE^2) analysis of material failure in cement/aggregate type
676 composites structures, *Proceedings of EURO-C 2014,* edited by N. Bicanic et al.,
677 published by CRC Press, pp. 39-49, 2014.
678 10. Unger, J.F., Hierarchical multi-scale models for localization phenomena withing the
679 framework of FE^2-X^1, *Proceedings of EURO-C 2014,* edited by N. Bicanic et al.,
680 published by CRC Press, pp. 75-85, 2014.
681 11. Dunn, K. Response Surface Methods, *Process Improvement Using Data.* 250-65, Web.
682 12. Bentley, J. L., and Ottmann T. "Algorithms for reporting and counting geometric
683 intersections." *Computers, IEEE Transactions on* 100.9 (1979): 643-647.
684 13. Rossi, P., Wu, X., Probabilistic model for material behaviour analysis and appraisement
685 of concrete structures, *Magazine of concrete research* 44.161 (1992): 271-280.
686 14. Tailhan, J-L., Dal Pont, S. and Rossi, P., From local to global probabilistic modeling of
687 concrete cracking, *Annals of Solid and Structural Mechanics* 1.2 (2010): 103-115.
688 15. Rossi, P., et al., Scale effect on concrete in tension, *Materials and Structures* 27.8 (1994):
689 437-444.
690 16. Rossi, P., Ulm, F-J, Hachi, F., Compressive behaviour of concrete: physical mechanisms
691 and modeling, *Journal of Engineering Mechanics* 122.11 (1996): 1038-1043.
692 17. Lemaitre, J., Chaboche, J.L., Mechanics of solid materials. *Cambridge University press*,
693 Cambridge, 1994.

694 18. Rossi, P., Tailhan, J.L., Cracking of concrete structures: interest and advantages of the
695 probabilistic approaches. *In: Rilem international conference on numerical modelling*
696 *strategies for sustainable concrete structures, SSCS'2012. Aix-en-Provence, France*,
697 2012.
698 19. Jirasek, M., Zimmermann, T., Rotating crack model with transition to scalar damage. *J*
699 *Eng Mech* 124(3):277–284, 1998.
700 20. Rots, J.G., Nauta, P., Kuster, G.M.A., Blaauwendraad, J., Smeared crack approach and
701 fracture localization in concrete, *HERON* 30(1), 1985.
702 21. De Borst, R., Nauta, P., Non-orthogonal cracks in a smeared finite element model. *Eng*
703 *Comput* 2(1):35–46, 1985.
704 22. Jirasek, M., Damage and smeared crack models. *In: Hofstetter G, Meschke G (ed)*
705 *Numerical modeling of concrete Ann. Solid Struct. Mech. cracking. CISM International*
706 *Centre for Mechanical Sciences*, vol 532. Springer, Vienna, pp 1–49, 2011.
707 23. Meschke, G., Grasberger, S., Becker, C., Jox, S., Numerical modeling of concrete
708 cracking. *Springer, chap Smeared Crack and X-FEM Models in the Context of*
709 *poromechanics*, pp 265–327, 2011.
710 24. Bazant, Z., Oh, B., Crack band theory for fracture of concrete. *Mater struct* 16(3):155–
711 177, 1983.
712 25. Feller, W., An introduction to probability theory and its applications, *vol 2. Wiley, New*
713 *York*, 2008.
714 26. Irwin, G., Linear fracture mechanics, fracture transition, and fracture control. *Eng Fract*
715 *Mech* 1(2):241–257, 1968.
716 27. Rossi, P., Comportement dynamique des bétons: du matériau à la structure. *Annales de*
717 *l'Institut technique du bâtiment et des travaux publics*. No. 511. Institut technique du
718 bâtiment et des travaux publics, 1993 5 (in french).

28. Lundgren K., Bond between ribbed bars and concrete. Part 1: Modified model, *Magazine of Concrete Research*, 57 (7) (2005): 371-382.
29. Rossi, P., Fissuration du béton : du matériau à la structure. Application de la mécanique linéaire de la rupture. PhD Thesis, Ecole Nationale des Ponts et Chaussées, p. 228, 1986 (in french), published in *rapport de recherche des LPC*, n°150, 1988 (in french).
30. Rossi, P., Coussy, O., Boulay, C., Acker, P., Comparison between plain concrete toughness and steel fibre reinforced concrete toughness, *Cement and Concrete Research*, vol. 16, pp. 303-313, 1986.
31. Rossi, P., Coupling between the crack propagation velocity and the vapour diffusion in concrete. *Materials and Structures*, vol. 22, pp. 91-97, 1989.

List of tables

Tables

Table 1

Material	Parameter	Value	Unit
Concrete	**Tensile strength (Weibull distribution)**		MPa
	Scale parameter	8.0	
	Shape parameter	1.0	
	dissipated energy G_c (lognormal distribution)		
	Mean value	1.3	10^{-4}MN mm^{-2}
	Deviation	8.4	10^{-4}MN mm^{-2}
	Compressive strength	55	MPa
	Young modulus	35000	MPa
Steel	**Young modulus**	191000	MPa
	Elastic limit	400	MPa

744 Table 2

745

ERC Type	Parameter	Symbol	Value (MPA)
ERC5	Tensile strength	σ_t^{cri}	
	Mean	$\mu_{\sigma_t^{cri}}$	3.2
	Deviaion	$\sigma_{\sigma_t^{cri}}$	0.4
	Tensile recovery	σ_r	1.3
	Residual stiffness	E_1'	
	Mean	$\mu_{E_1'}$	1000.
	Deviation	$\sigma_{E_1'}$	50.
ERC10	Tensile strength	σ_t^{cri}	
	Mean	$\mu_{\sigma_t^{cri}}$	3.05
	Deviaion	$\sigma_{\sigma_t^{cri}}$	0.4
	Tensile recovery	σ_r	0.75
	Residual stiffness	E_1'	
	Mean	$\mu_{E_1'}$	390.
	Deviation	$\sigma_{E_1'}$	50.
ERC20	Tensile strength	σ_t^{cri}	
	Mean	$\mu_{\sigma_t^{cri}}$	3.4
	Deviaion	$\sigma_{\sigma_t^{cri}}$	0.6
	Tensile recovery	σ_r	0.75
	Residual stiffness	E_1'	
	Mean	$\mu_{E_1'}$	550.
	Deviation	$\sigma_{E_1'}$	100.

746

747 $\mu_{\sigma_t^{cri}}$,$\sigma_{\sigma_t^{cri}}$, are the parameters of the lognormal distribution function of the tensile strength,
748 and $\mu_{\mathrm{E}_1'}$, $\sigma_{\mathrm{E}_1'}$, are the parameters of the lognormal distribution function of the residual
749 stiffness after cracking.

750

751

752

753

754

755

756 Table 3

Cohesion	$\boldsymbol{C}$	10	$\boldsymbol{MPa}$
Critical tangent displacement	δ_t^{cri}	4	$10^{-6}m$

757

758

759 Table 4

Model used	**Calculation time (sec)**	**Number of elements in the reinforced zone**	**Number of nodes in the reinforced zone**
Local	4750	2318	1398
Macro-ERC1	527	1125	1480
Macro-ERC2	1220	2057	2592
Macro-ERC3	520	625	888

760

List of figures

784 Fig.19. Crack mouth opening displacement (CMOD) versus loading curves (DCB specimen)
785 related to ERC3
786 Fig.20. Example of cracking pattern of the DCB specimen obtained with 3D simulations –
787 Macroscopic model
788 Fig.21. 2D Finite elements mesh related to the local approach
789 Fig.22. Crack mouth opening displacement (CMOD) versus loading (DCB specimen) related
790 to the local approach
791 Fig.23. Example of cracking pattern of the DCB specimen obtained with 2D simulations –
792
793

Figures

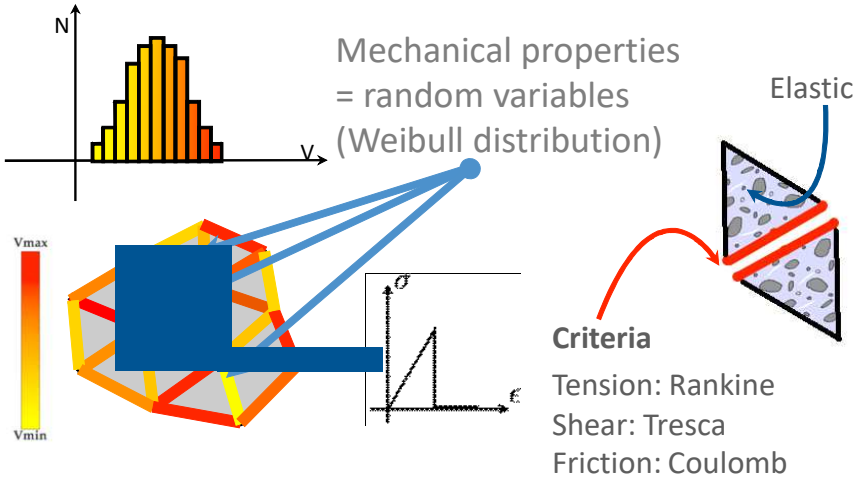

Fig.1

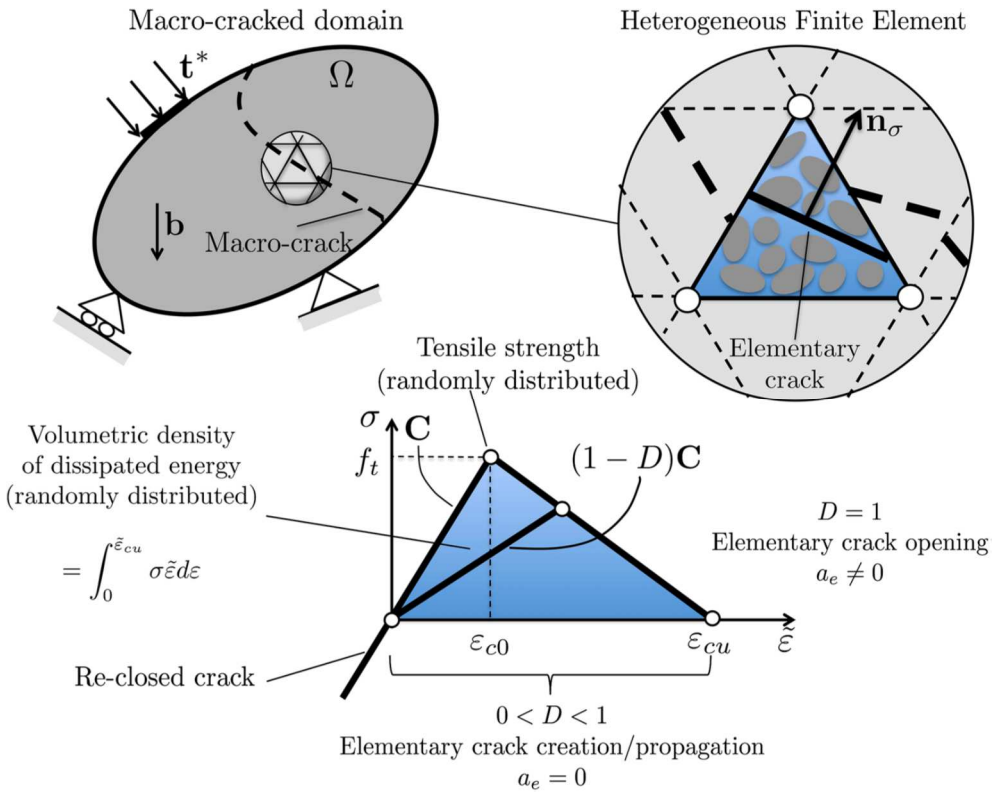

Fig. 2

800

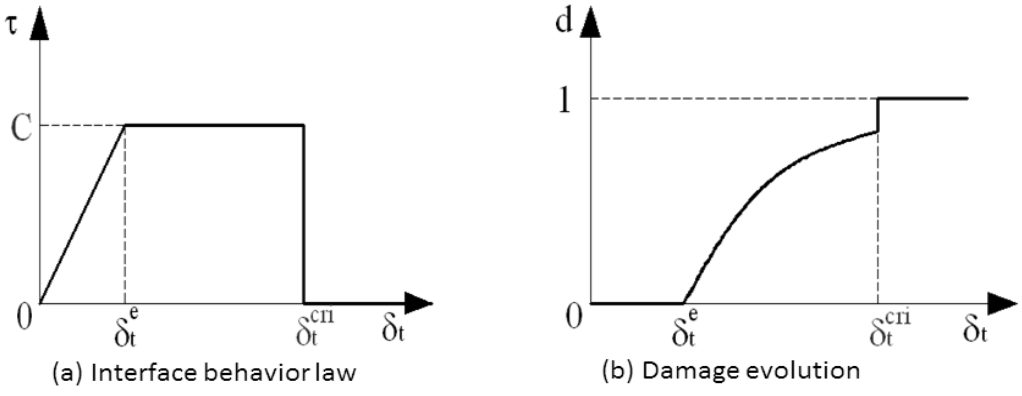

801

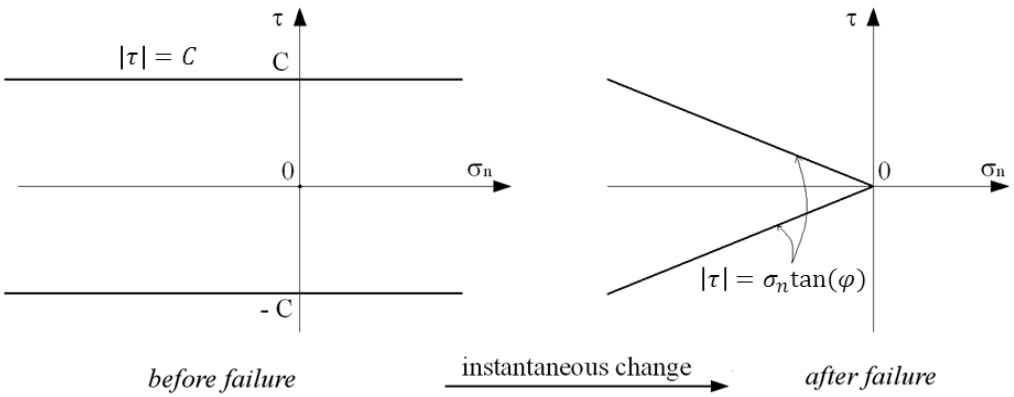

802

803 Fig.3

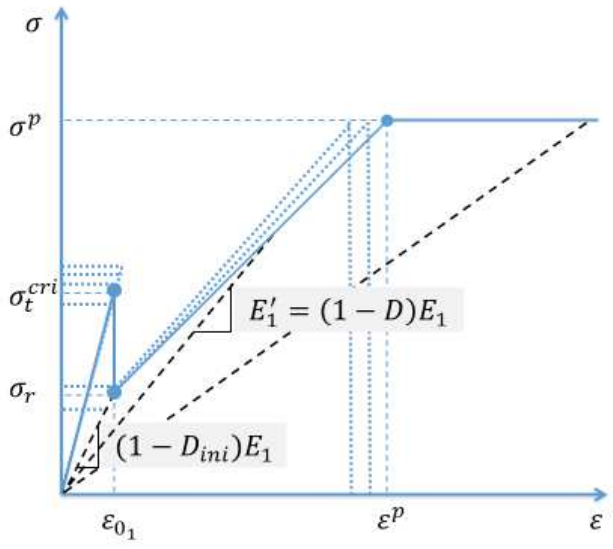

804

805 Fig.4

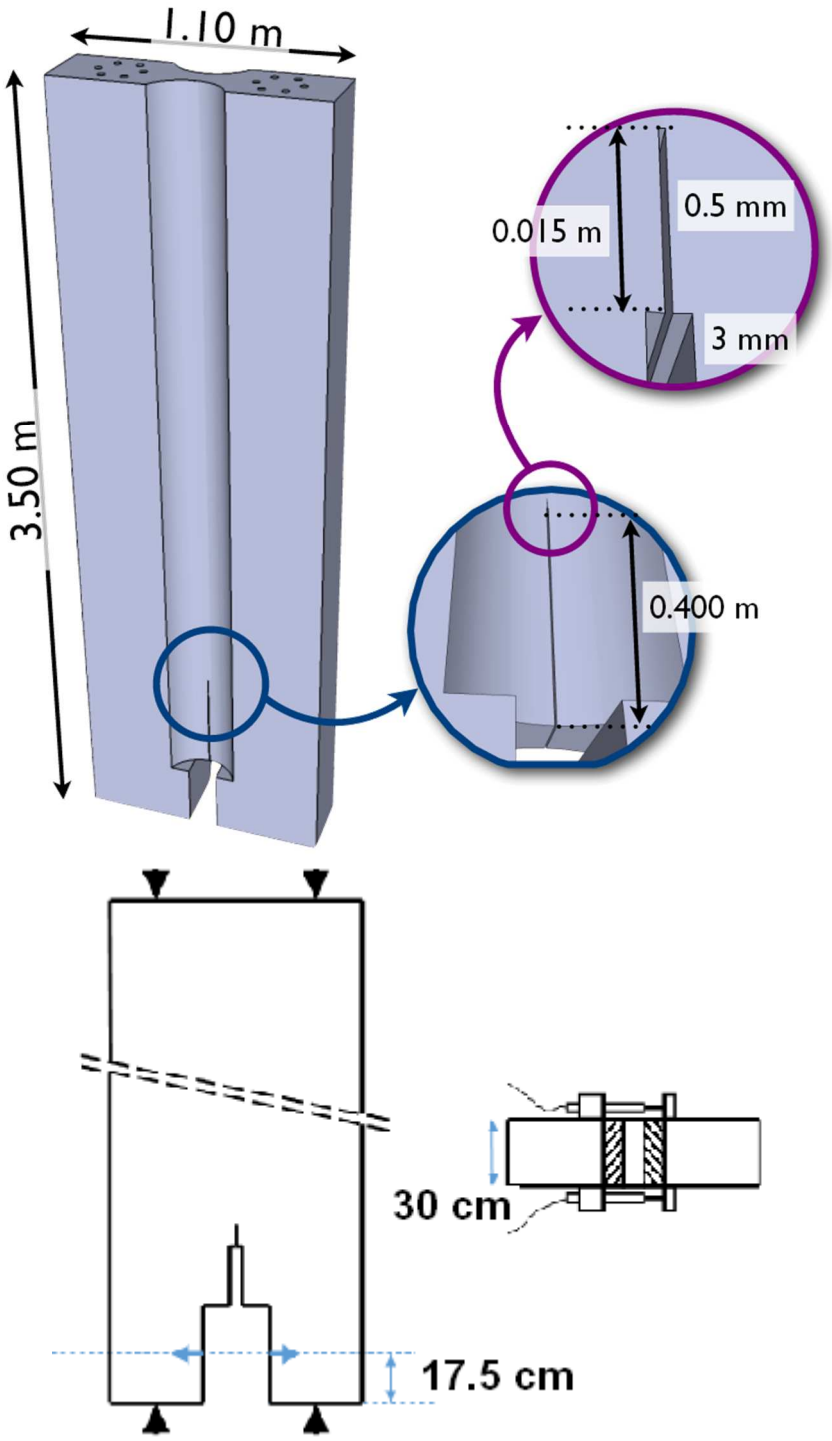

Fig.5

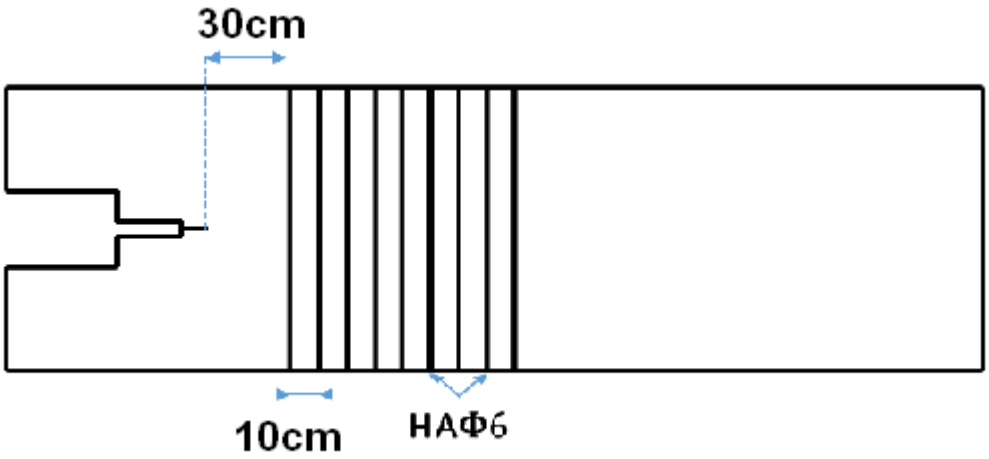

813

814 Fig.6

815

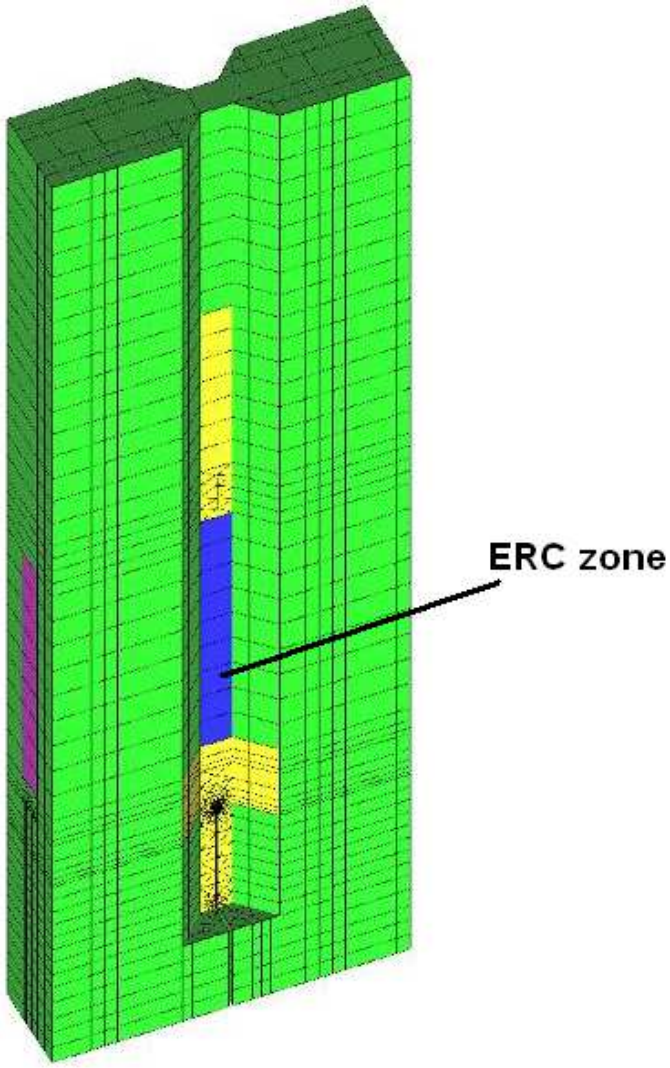

816

817 Fig.7

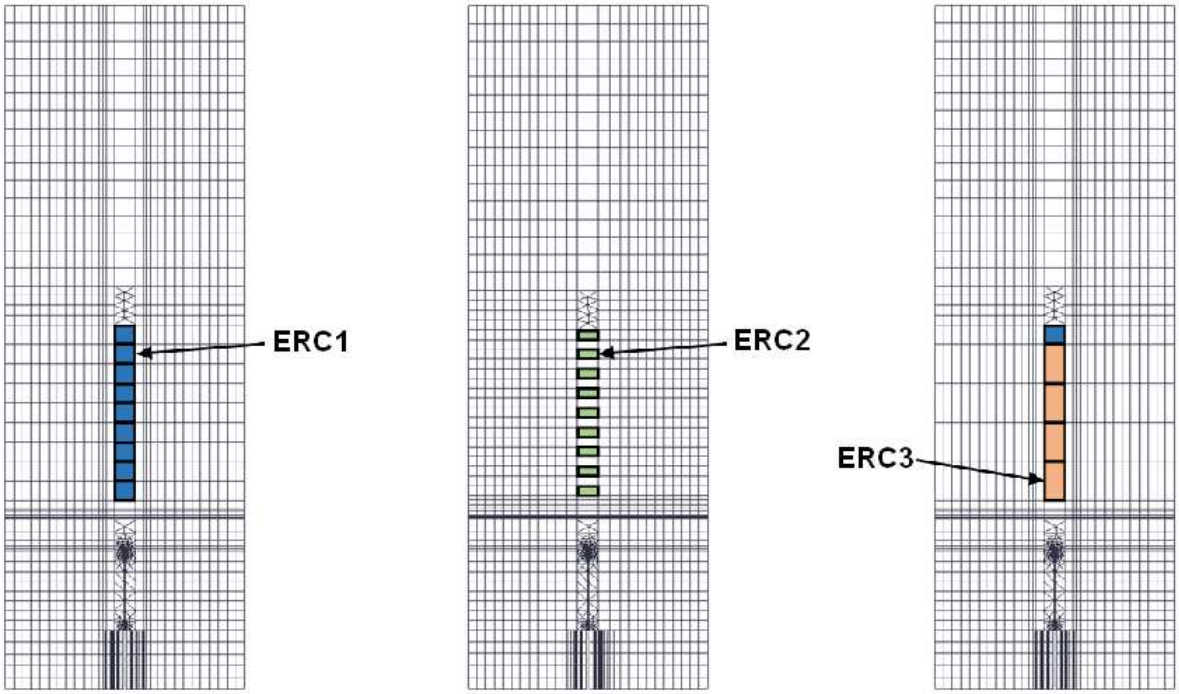

818

819 Fig. 8

820

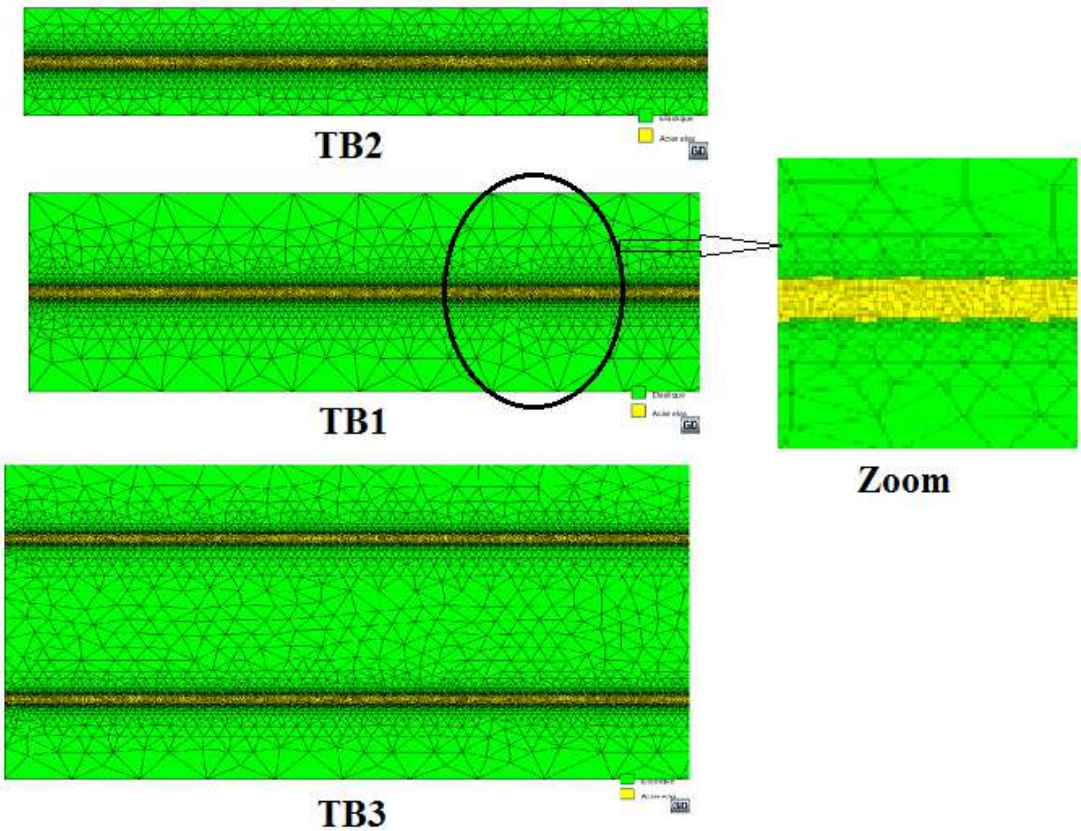

821

822 Fig.9

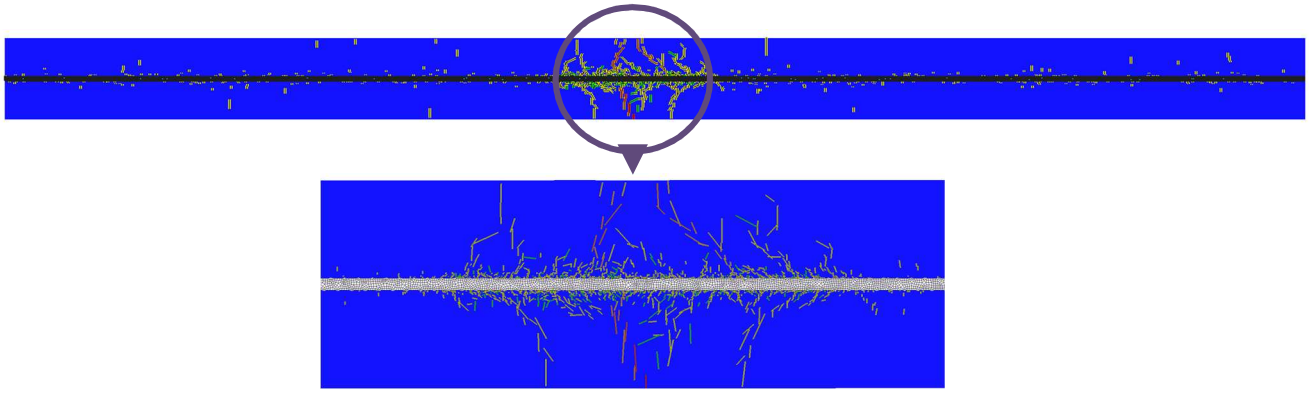

Fig. 10

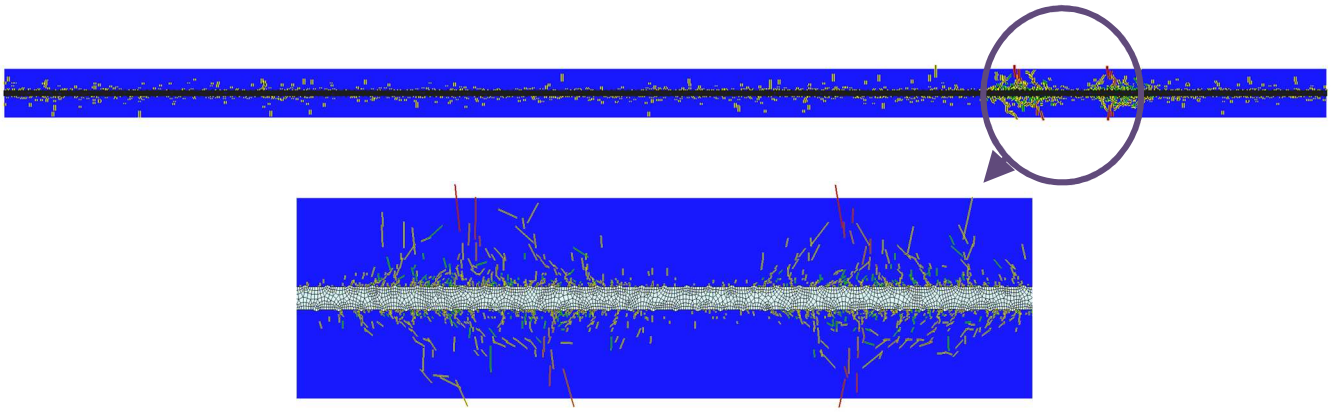

Fig.11

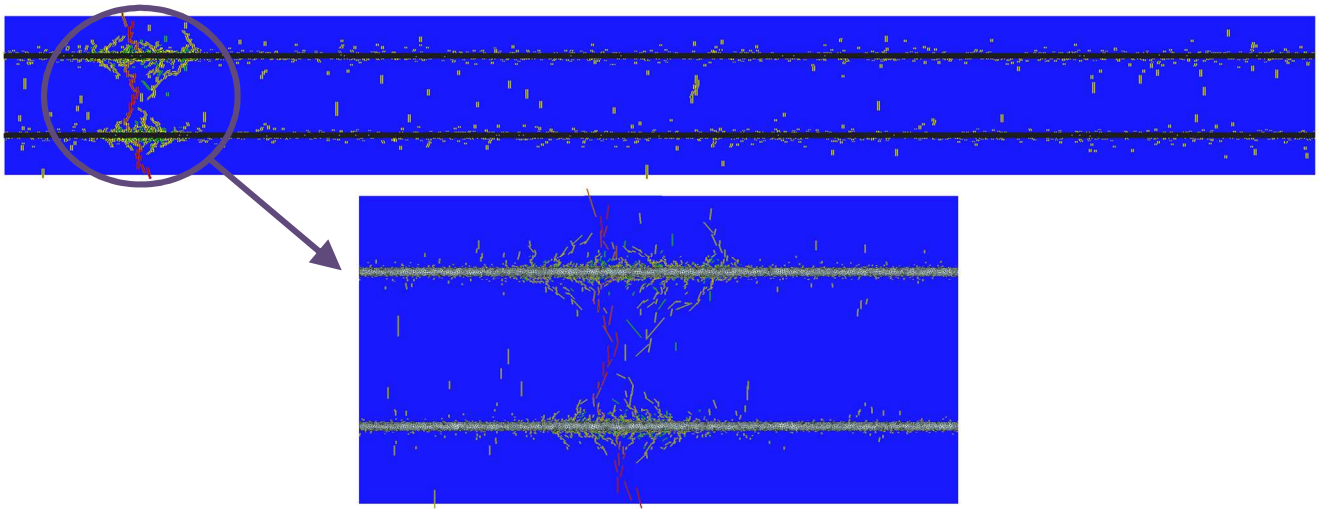

Fig.12

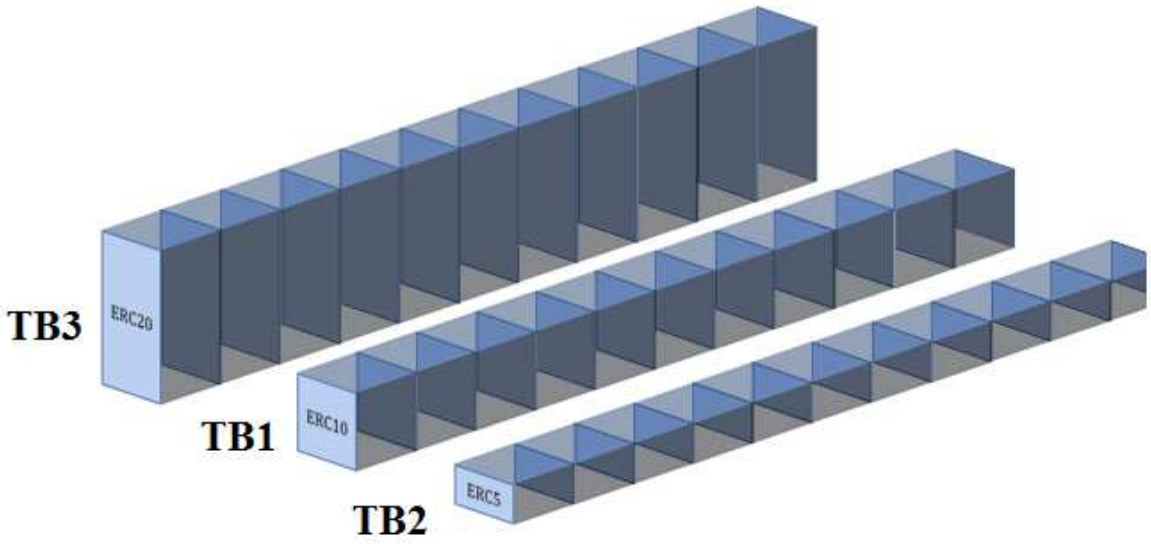
TB3
ERC20
TB1
ERC10
TB2
ERC5

Fig.13

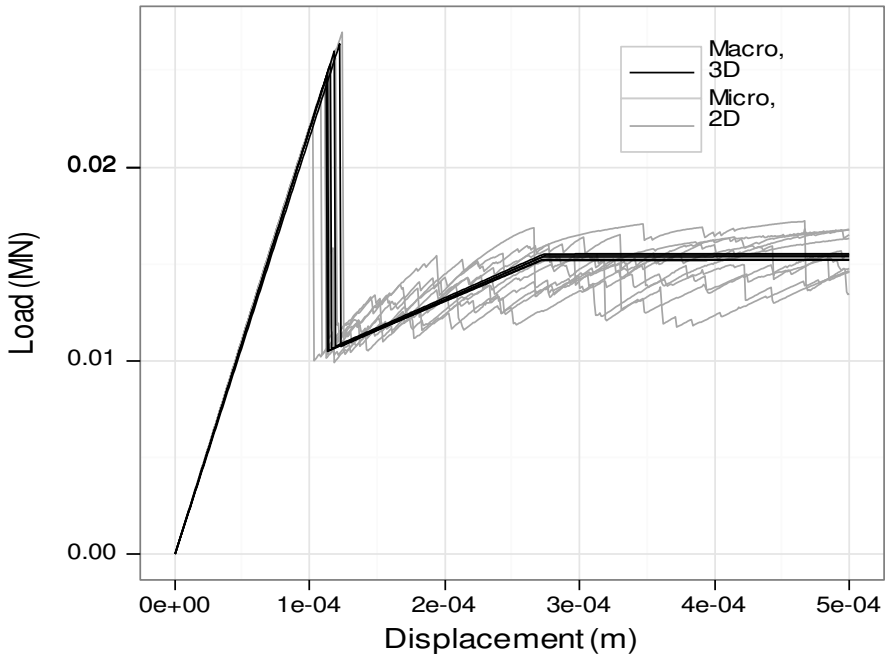
Macro, 3D
Micro, 2D
0.02
0.01
0.00
Load (MN)
0e+00
1e-04
2e-04
3e-04
4e-04
5e-04
Displacement (m)

Fig. 14

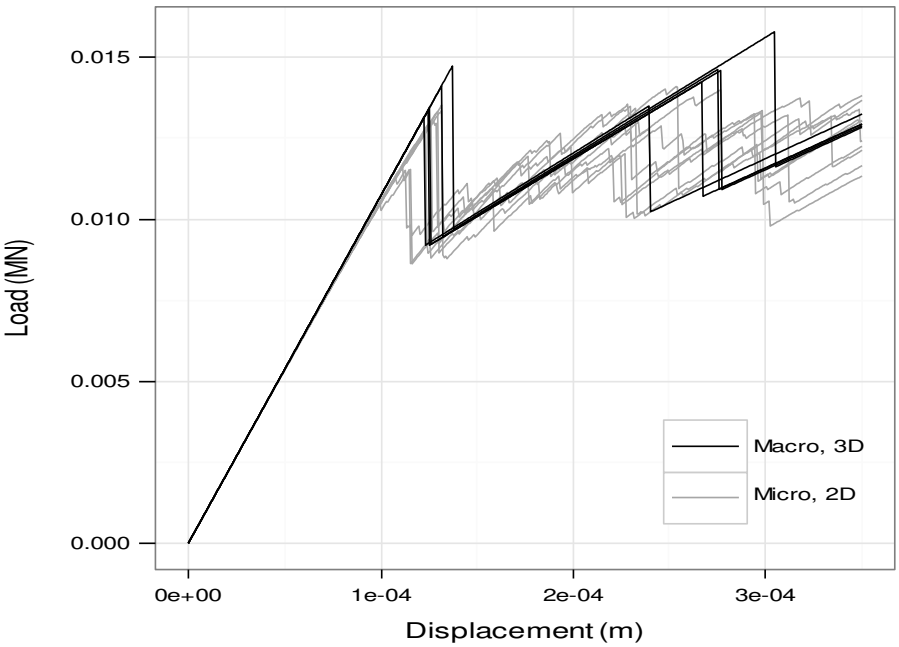

860

861 Fig. 15

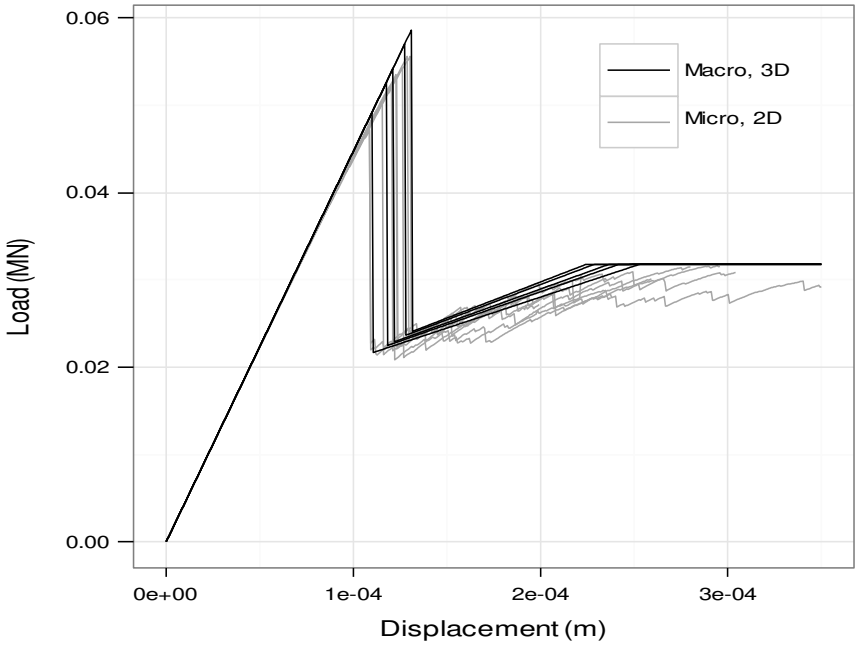

862

863 Fig. 16

864

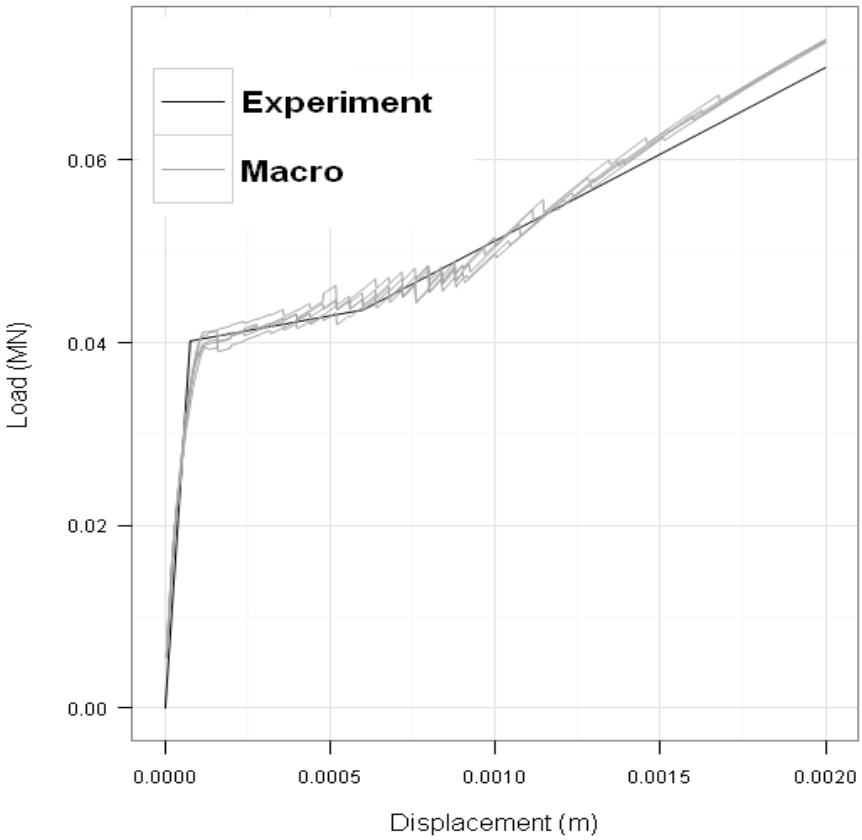

865

866 Fig. 17

867

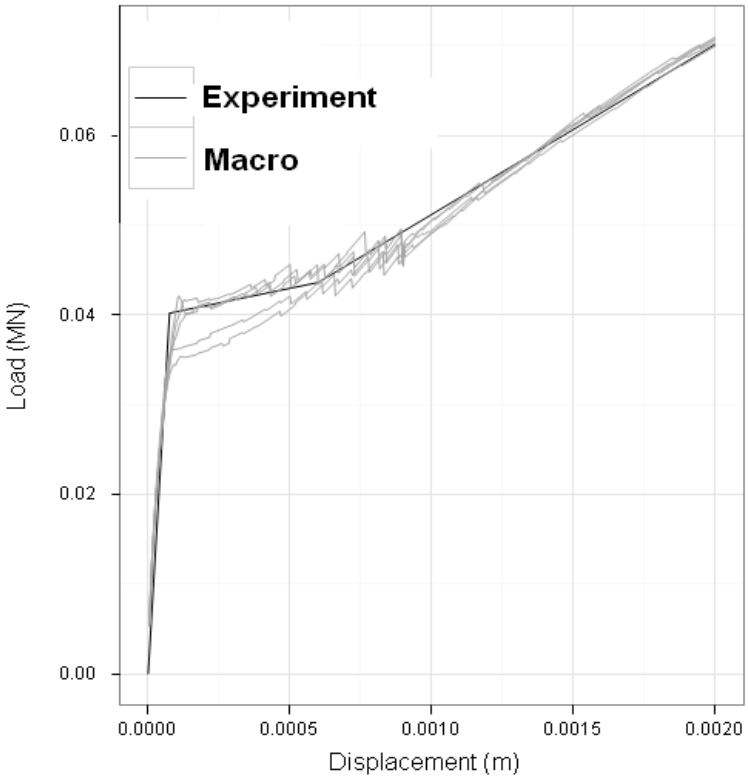

868

869 Fig. 18

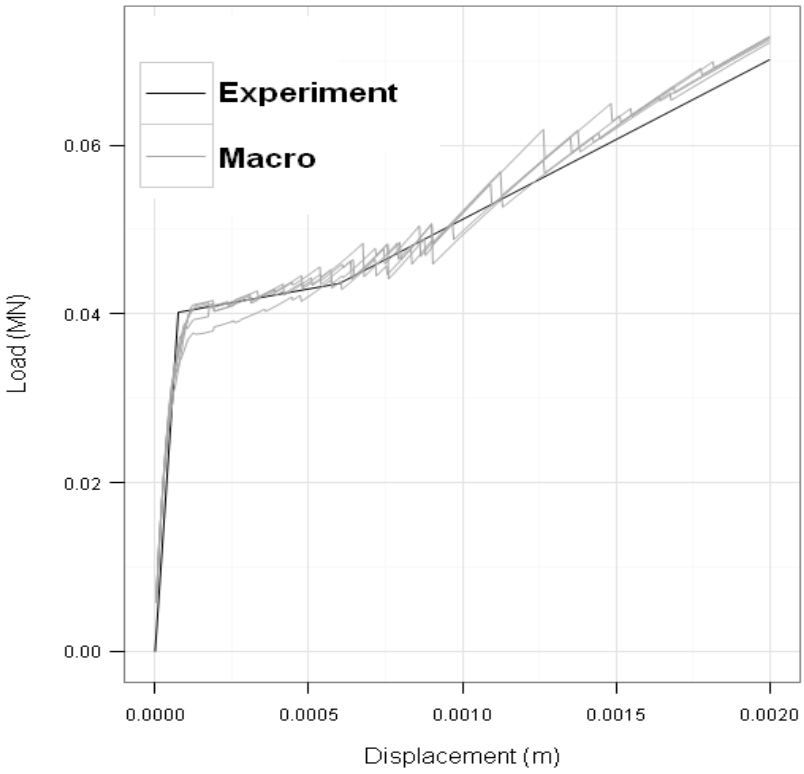

870

871 Fig. 19

872

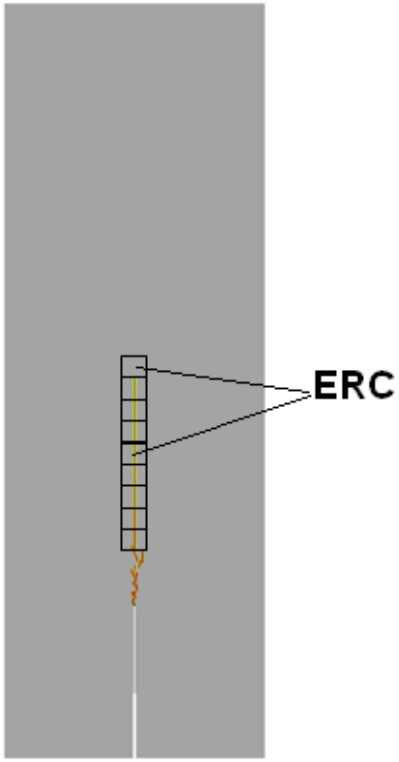

873

874 Fig. 20

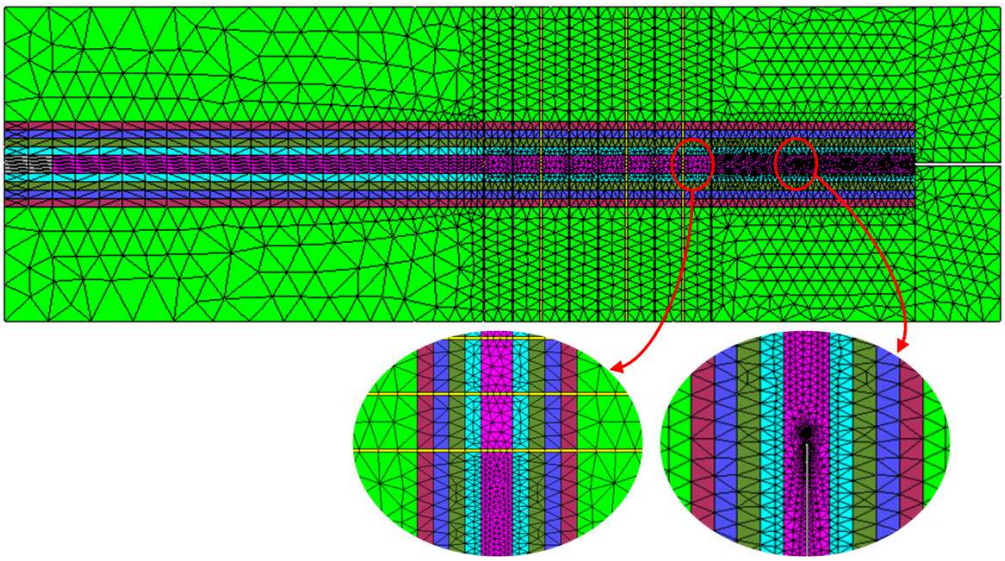

875

876 Fig. 21

877

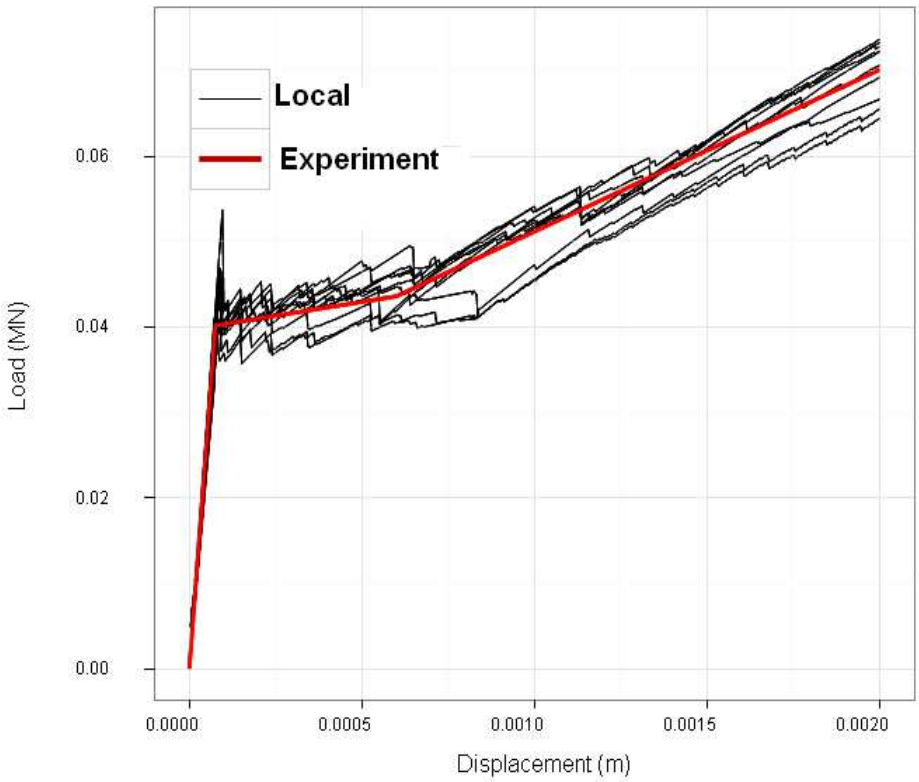

878

879 Fig. 22

880

881

882

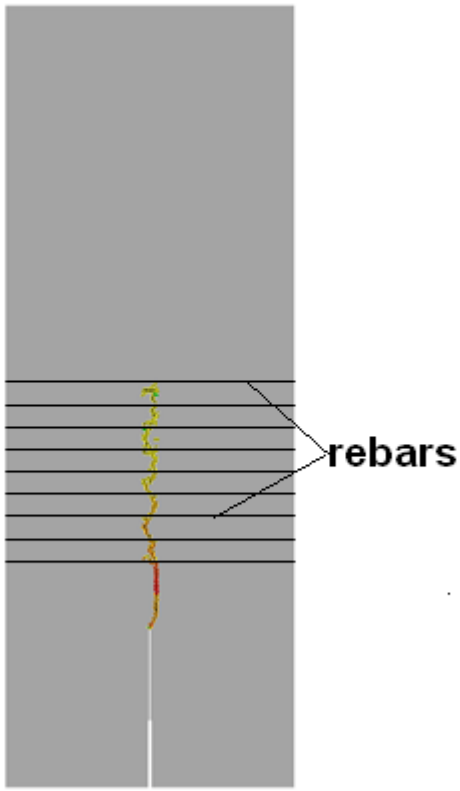

883

884 Fig.23